analytical chemistry

pubs.acs.org/ac Article

Quantitative Feedback Referencing for Improved Kinetic Fitting of Scanning Electrochemical Microscopy Measurements

Sebastian Amland Skaanvik, Lisa Irene Stephens, Samantha Michelle Gateman, Matthias Geissler, and Janine Mauzeroll*

Cite This: *Anal. Chem.* 2022, 94, 13852−13859 Read Online

ACCESS | Metrics & More | Article Recommendations | Supporting Information

ABSTRACT: Scanning electrochemical microscopy (SECM) has matured as a technique for studying local electrochemical processes. The feedback mode is most commonly used for extracting quantitative kinetic information. However, approaching individual regions of interest, as is commonly done, does not take full advantage of the spatial resolution that SECM has to offer. Moreover, fitting of experimental approach curves remains highly subjective due to the manner of estimating the tip-to-substrate distance. We address these issues using negative or positive feedback currents as a reference to calculate the tip-to-substrate distance directly for quantitative kinetic fitting of approach curves and line profiles. The method was first evaluated by fitting simulated data and then tested experimentally by resolving negative feedback and intermediate kinetics behavior in a spatially controlled fashion using (i) a flat, binary substrate composed of Au and SiO_2 segments and (ii) a dual-mediator system for live-cell measurements. The methodology developed herein, named quantitative feedback referencing (QFR), improves fitting accuracy, removes fitting subjectivity, and avoids substrate−microelectrode contact.

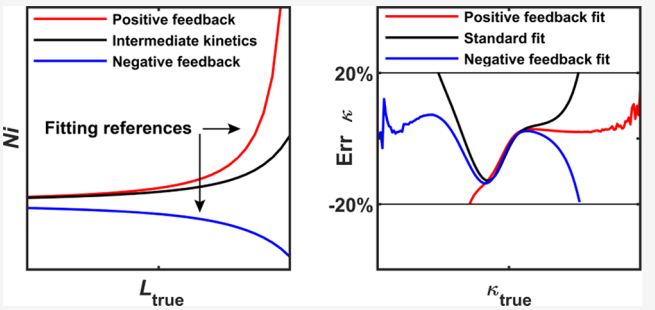

Downloaded via WESTERN UNIV on March 29, 2023 at 19:16:49 (UTC).
See https://pubs.acs.org/sharingguidelines for options on how to legitimately share published articles.

INTRODUCTION

Scanning electrochemical microscopy (SECM) was introduced in 1989[1] and is the most widely used electrochemical scanning probe method for measuring electrochemical activity.[2] SECM has been applied to many research areas to understand local electrochemical reactivity related to corrosion,[3,4] energy conversion,[5−7] transport and reaction kinetics,[8−10] and cellular redox activity.[11−13] Of the different SECM operational modes, including generation−collection mode,[14] shielding/redox competition mode,[15,16] and distance/potential modulation mode,[17,18] the feedback mode is most commonly employed due to its versatility, high resolution, and ease of implementation.[2] The feedback mode operates using a redox mediator in the electrolyte that undergoes oxidation/reduction at the microelectrode, resulting in a faradaic current that is dependent on the topography and the electrochemical activity of the substrate toward the redox mediator. Three cases exist: (i) negative feedback, when the redox mediator is not regenerated at the substrate; (ii) positive feedback, when the redox mediator is instantaneously regenerated at the surface; and (iii) intermediate kinetics, where the rate of the redox mediator regeneration is somewhere in between negative and positive feedback. For the intermediate kinetics case, the kinetic rate constant at the surface can be determined at a specific location on the substrate by performing an approach curve, which is produced by measuring the current response during an approach towards the substrate. The experimental data is then fitted to analytical approximations to extract the kinetic rate constant for further analysis and comparison.[19−21] The fitting method requires the tip-to-substrate distance to be known, where a lack of accuracy can greatly affect fitting quality.[22]

There are four methods currently used to estimate the tip-to-substrate distance. The first method involves the use of an additional technique for measuring topography based on shearforce,[23−26] impedance (AC)-SECM,[17,27,28] intermittent contact (IC)-SECM,[29,30] or atomic force microscopy (AFM)-SECM,[31−33] which all have been previously demonstrated to track the tip-to-substrate distance independently. Existing methods can certainly circumvent problems arising from varying topography but require sophisticated instrumentation and can complicate experimental procedures, probe fabrication, and data interpretation. The second method relies on approximating the distance via collision, which involves intentionally making contact of the microelectrode with the substrate. Upon contact, an inflection in the current response is observed, which is then assumed to be the zero tip-to-substrate

Received: June 11, 2022
Accepted: September 13, 2022
Published: September 27, 2022

ACS Publications © 2022 American Chemical Society

https://doi.org/10.1021/acs.analchem.2c02498
Anal. Chem. 2022, 94, 13852−13859

distance. Often times, it is difficult to gauge where such inflection initiates, which introduces subjectivity in kinetic fitting. Furthermore, "crashing" the microelectrode into the substrate is not ideal as it can physically damage the microelectrode, sample, and lead to electrode fouling.[34] The third method is based on including the zero tip-to-substrate distance as an adjustable fitting parameter.[35,36] However, this method cannot cover the entire kinetic range and can obscure deviations from assumed kinetics.[22]

Alternatively, one can take advantage of the negative feedback response to deduce the tip-to-substrate distance, which are quantitatively related to each other. This positioning strategy was implemented already in 1991 by Unwin and Bard.[37] For example, Takahashi et al. introduced the voltage-switching mode for high-resolution topography and reactivity mapping of cells in a hopping mode regime using a dual-mediator system.[38] Lhenry et al. demonstrated that the irreversible redox mediator, anthracene, can be used to access negative feedback currents independent of surface properties.[39] Negative feedback can also be achieved spatially by having a sample embedded in the insulating material for probe positioning, as demonstrated by Souto et al., using oxygen as a mediator to probe the tip-to-substrate distance at a single point.[40] If fact, using a single-point analysis has attracted much attention as it allows for kinetic imaging in constant-plane mode.[41−43] Many strategies have been implemented to access the tip-to-substrate distance using negative feedback, but there are no studies on the accuracy of calculating the tip-to-substrate distance in this way and how such errors propagate during kinetic fitting, especially when a single point is used. Moreover, kinetic fitting can be highly subjective to experimental errors as well.[44]

In this work, we evaluate using negative and positive feedback currents as a quantitative reference for fitting kinetics, named herein quantitative feedback referencing (QFR). The method use negative or positive feedback currents to calculate the tip-to-substrate distance on a point-by-point basis, which can then be used directly for kinetic fitting, circumventing the use of the microelectrode area and piezo extension in the fitting process. Exemplified using available analytical approximations, this fitting method was validated and found to improve fitting quality and robustness toward experimental errors. A thorough single-point accuracy analysis was carried out in this framework to validate single-point and constant-plane imaging strategies for determining the tip-to-substrate distance/topography and kinetics. We demonstrate the success of this analysis for two different experimental scenarios: (i) by performing line scans over an electrically insulating substrate that is in plane with a kinetically limited region (i.e., flat), and (ii) by utilizing a dual-mediator system where one species is not electrochemically reactive toward the cell membrane of live cells (i.e., biological substrates).

EXPERIMENTAL SECTION

Numerical Simulations. Finite element modeling (FEM) was carried out using COMSOL Multiphysics Software version 5.3a (COMSOL, Burlington, MA, US) for an oxidation occurring at the electrode surface. Concentration profiles of redox species were simulated using the module Transport of Diluted Species. Mass transport to the electrode was calculated according to Fick's law, and the diffusion coeffcient of oxidized and reduced species (D) was chosen to be 6.7×10^{-10} m^2 s^{-1}, corresponding to that of ferrocenemethanol (FeMeOH) in water at 25 °C.[45] A detailed description of the simulation parameters and mesh is provided in the Supporting Information (Sections S1−S3).

Materials and Reagents. All redox mediators, hexaammineruthenium(III) chloride ($Ru(NH_3)_6Cl_3$, 99% purity, referred herein to as Ruhex), and FcMeOH (97% purity) as well as electrolyte and buffer reagents were purchased from Sigma-Aldrich (Oakville, ON, Canada). All solutions were prepared using deionized water from a Milli-Q water purification system (18.2 MΩ cm resistivity; MilliporeSigma, Oakville, ON, Canada).

SECM Using a Single Redox Mediator: over Au/SiO_2 Substrates. Au/SiO_2 substrates were fabricated according to previously reported methods.[46] A 11 μm carbon-fiber microelectrode (C-UME, RG = 2, RG = $\frac{r}{a}$, Figure 1A) was fabricated in-house as described previously[47] and polished with lapping film. A solution of 1 mM Ruhex in 0.1 M KCl was used as a redox mediator for imaging. A three-electrode setup including a Ag/AgCl quasi reference electrode and a Pt wire

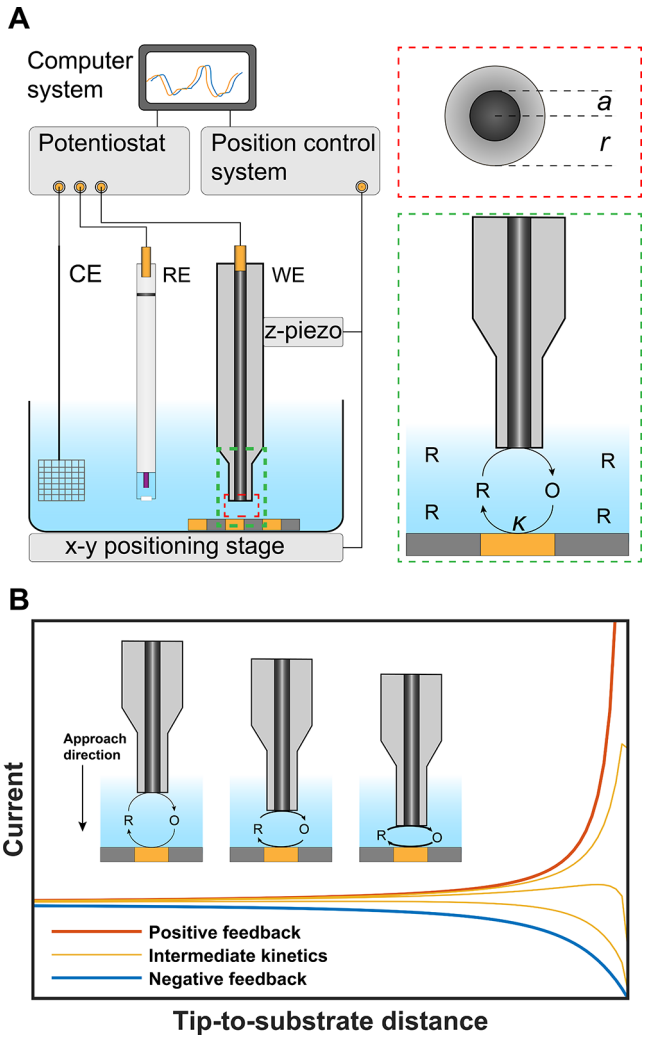

Figure 1. (A) Scheme showing the experimental setting for SECM feedback mode measurements. (B) Scheme and plot of approach curves, showing negative feedback ($\kappa = 0$), positive feedback $\kappa = \infty$, and intermediate kinetics ($\kappa > 0, < \infty$). The inset describes the increased flux from the regeneration process at the surface during an approach curve.

https://doi.org/10.1021/acs.analchem.2c02498
Anal. Chem. 2022, 94, 13852−13859

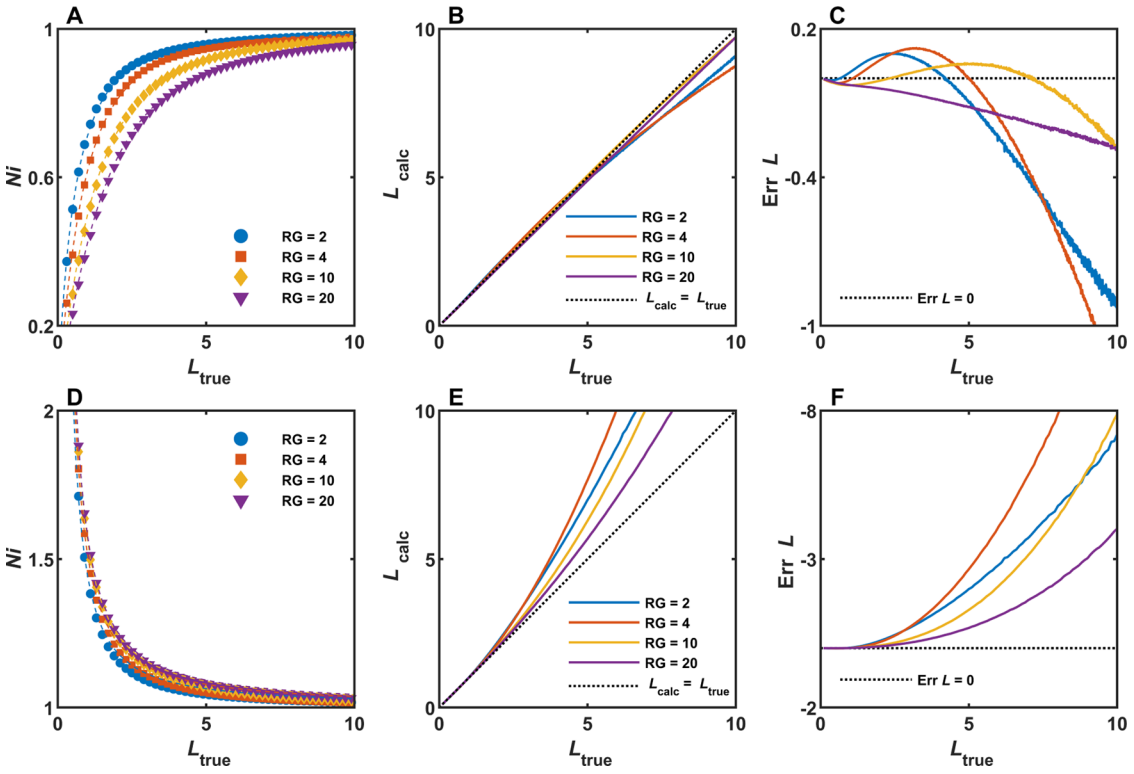

Figure 2. (A) Plot of simulated negative feedback approach curves for different values of RG (markers), compared to the analytical approximation (dashed lines). (B) Plot of the calculated normalized tip-to-substrate distance (L_{calc}) vs the true normalized tip-to-substrate distance (L_{true}) from panel (A). (C) Plot of Err L vs L_{true} from panel (B). (D) Plot of simulated positive feedback approach curves for different values of RG (markers), compared to the analytical approximation (dashed lines). (E) Plot of the calculated normalized tip-to-substrate distance (L_{calc}) vs the true normalized tip-to-substrate distance (L_{true}) from panel (D). (F) Plot of Err L vs L_{true} from panel (E).

counter electrode was used. Imaging was carried out at −350 mV vs Ag/AgCl at a scan rate of 1 μm s^{-1}. All SECM experiments were conducted using an ElProScan 3 system equipped with a Bipotentiostat/Galvanostat PG 340 (HEKA Elektronik GmbH, Reutlingen, Germany).

SECM Using Double Redox Mediators: over a Biological Sample. Zeonor 1060R disks (2.3 cm in diameter and 0.5 mm in thickness) were fabricated and treated with oxygen plasma as described previously.[48] Human embryonic kidney cells HEK293 (3.5×10^5 cells; generously donated by Susan Cole, Queen's University, Kingston, ON, Canada) were seeded on a Zeonor disk 2 days before SECM experiments. The disk was washed with phosphate-buffered saline (PBS, pH 7.4) twice before being mounted into the electrochemical cell. The substrate was then covered with 2 mL of imaging solution containing 0.5 mM Ruhex, 0.5 mM FcMeOH, and 25 mM 2-[4-(2-hydroxyethyl)piperazin-1-yl]ethane-1-sulfonic acid (HEPES) in Dulbecco's modified Eagle's medium (DMEM). A 7 μm C-UME (RG = 4) was first positioned over the cells through negative feedback of Ruhex reduction. Then, the electrode was retracted 350 μm ($L \approx 100$) away from the sample, and a 10 s chronoamperometry measurement was performed in the bulk solution for FcMeOH at 350 mV vs Ag/AgCl to obtain the bulk steady-state current. The electrode was then moved down 350 μm and an approach curve was recorded at 350 mV at 0.5 μm s^{-1} (12 μm in total). After the approach curve was complete, the potential was switched to −350 mV for Ruhex and the approach curve was performed by retracting the electrode 12 μm at 0.5 μm s^{-1}. The electrode was again retracted 350 μm in the z-direction, and a 10 s chronoamperometry measurement was performed for Ruhex at −350 mV.

RESULTS AND DISCUSSION

Validation of Tip-to-Substrate Distance Determination by Simulating Approach Curves. This section describes the validation and accuracy of calculating the normalized tip-to-substrate distance, L, from negative and positive feedback approach curves for intermediate kinetics analysis and accurate microelectrode positioning. L is defined herein as, $L = \frac{d}{a}$, where d is the tip-to-substrate distance, and a is the radius of the electroactive area of a disk microelectrode (Figure 1A). We simulated approach curves with different RG values and a known normalized tip-to-substrate distance, L_{true}, where Figure 2A,D shows that the simulated data (markers) agrees well with the analytical approximations for a disk electrode (dashed lines, Section S4).[20,21] We then calculated the normalized tip-to-substrate distance (L_{calc}) by fitting the simulated approach curves for L to the analytical approximation at each point along the approach curve using a least squares fitting method (Section S5). The accuracy of the fitting for is evaluated by considering the error in L (Err L), defined as

$$\text{Err } L = L_{calc} - L_{true} \quad (1)$$

For negative feedback, the dependence of L_{calc} and Err L on L_{true} is shown in Figure 2B,C, demonstrating that L can be accurately calculated from a single point in the approach curve. The accuracy is lowest when L_{true} is large, as the current reaches its bulk value, $Ni = 1$. Closer to the surface, when L_{true}

https://doi.org/10.1021/acs.analchem.2c02498
Anal. Chem. 2022, 94, 13852−13859

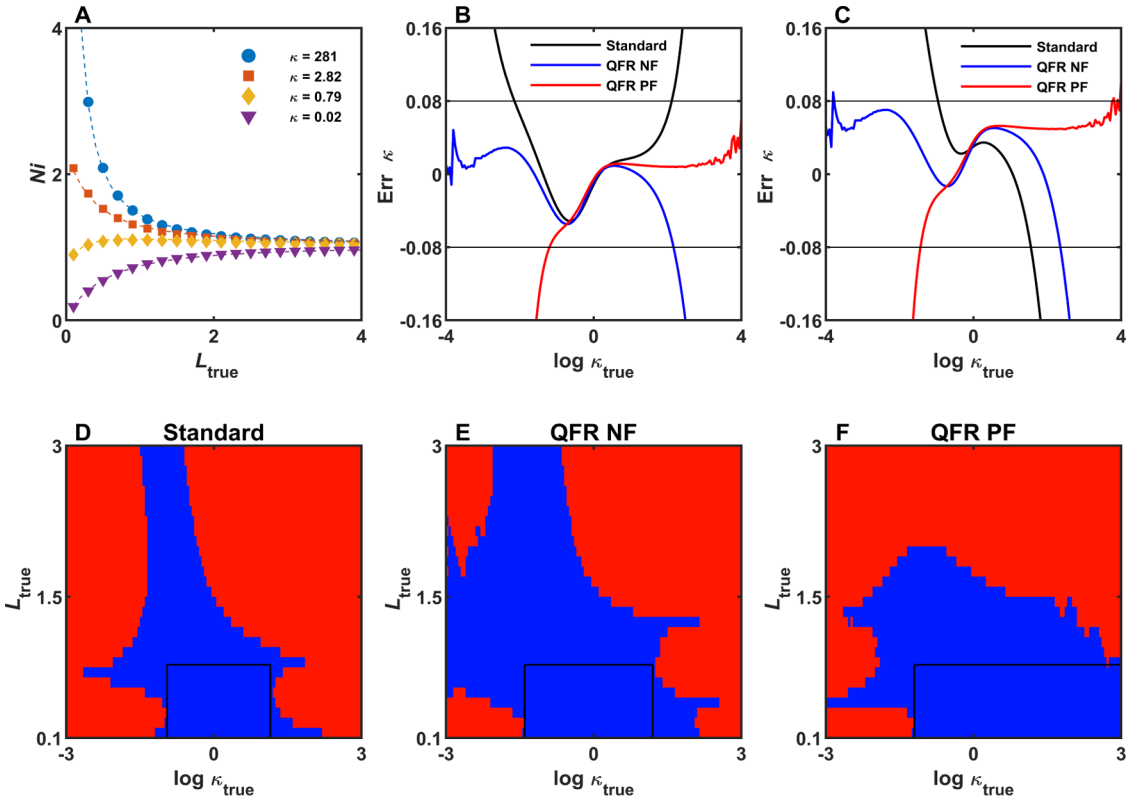

Figure 3. (A) Plot of simulated approach curves for different values of κ_{true} (markers) compared to the analytical approximations (dashed lines). (B) Plot of Err κ vs log κ_{true} for fitting entire approach curves to the analytical approximations (L_{true} = [0.1,10]). (C) Plot of Err κ vs log κ_{true} for fitting entire approach curves to the analytical approximations with a 10% error in the microelectrode area radius (L_{true} = [0.1,10]). (D−F) Logic plots for the standard method and QFR for negative (NF) and positive feedback (PF), respectively, showing whether a single point is sufficient for fitting κ with an accuracy better than 20%.

$\leq$ 5, the accuracy is excellent, |Err L| < 0.13. For positive feedback, good accuracy is achieved for $L_{true} \leq 2$, |Err L| < 0.25, as seen in Figure 2E,F. Further away from the surface, $L_{true} > 2$, large errors can occur if attempting to calculate L from a single point of positive feedback current. When the goal is to accurately position the microelectrode at a distance far away from the surface, the best strategy is to make the current measurement close to the surface before repositioning to the desired height. Note that the L calculation can be carried out before the experiment for consistent positioning. Complete accuracy ranges are reported in the Supporting Information (Sections S6 and S7). A thorough analysis of the accuracy of calculating L from a single point has been carried out and validated previous microelectrode positioning strategies, providing an alternative way of acquiring the tip-to-substrate distance for kinetic fitting.

Validation of Quantitative Feedback Referencing. The accuracy of the QFR method was studied using the feedback mode, which generally relies on irreversible first-order kinetics to determine electrochemical reactivity of electrodes,[35] ion-exchange materials,[49] and enzyme layers.[50] We simulated approach curves with varying kinetic rate constants (k, Figure 3A, markers). The kinetic rate constants are normalized with respect to a and D to describe the general case, $\kappa = \frac{ka}{D}$. Simulated approach curves were in good agreement with the analytical approximation (Figure 3A, dashed lines, Section S4).[19] To evaluate the fitting procedure, the error in κ was defined as

$$\text{Err } \kappa = \log \frac{\kappa_{calc}}{\kappa_{true}} \tag{2}$$

where κ_{calc} is the calculated and κ_{true} is the defined value of κ. The accuracy of fitting entire approach curves to obtain a single value of κ_{calc} was explored using both L_{true} and L_{calc} (Section S8-S10). We found that QFR improves the range where κ can be fitted with an accuracy better than 20% for both negative and positive feedback as a reference (RG = 2, Figure 3B). The accurate ranges for QFR are slightly shifted toward their respective limiting cases; negative feedback referencing is more accurate for fitting approach curves where κ is low and vice versa. This occurs because using L_{calc} corrects for the errors in the equations for negative (or positive) feedback, which are used as a basis for describing the intermediate kinetic case (Section S4). The improved fitting accuracy is most substantial for low RG values, which are advantageous as these UMEs are less likely to crash during imaging and have higher current sensitivity.[51] We demonstrate that QFR improves the fitting of entire approach curves, even relative to the ideal case where the tip-to-substrate distance and electrode area are known with 100% accuracy, which QFR does not use directly.

Deviations from the assumed experimental conditions, coplanar microelectrode/substrate, microelectrode area, and geometry can have an influence on data interpretation. Especially, error in the microelectrode area can have a large effect as it is used to construct the Ni-L relationship, which can lead to error propagation.[44] To demonstrate how QFR can improve fitting in such scenarios, a 10% error in the

https://doi.org/10.1021/acs.analchem.2c02498
Anal. Chem. 2022, 94, 13852−13859

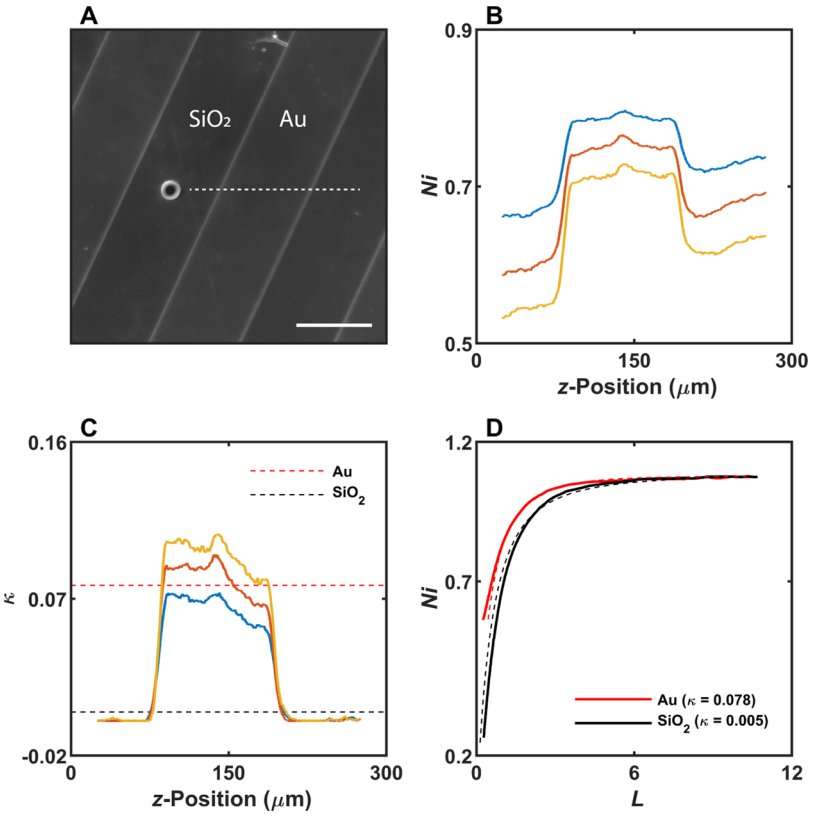

Figure 4. (A) Optical microscopy image of a Au/SiO_2 substrate treated with 1-hexanethiol (view from below). The UME is positioned over a SiO_2 strip which appears slightly darker than the adjacent SAM-covered Au regions. Scale bar: 100 μm. (B) Line scans at different heights over the Au/SiO_2 substrate. (C) Single-point κ-fitting for the line scans in panel (B) using the negative feedback region for calculating the tip-to-substrate distance. (D) Approach curves and fitted curves over the Au (red line, κ = 0.078) and SiO_2 (black line, κ = 0.005) regions, respectively.

microelectrode area was introduced such that the microelectrode was 10% smaller than expected. The resulting Err κ, evaluated based on absolute rate constants in this case, is shown in Figure 3C, where the accuracy range for QFR is unaffected and the standard method is substantially affected. This can be rationalized as the error is introduced for the QFR method only in the last step when the absolute rate constant is calculated, which translates the error plots on the y-axis. The accuracy ranges for different RG values are reported in the Supporting Information (Section S11 and S12). If the kinetic rate constant can be determined from a single point, it would offer the possibility to extend kinetic analysis into the $x-y$ plane by fitting constant-plane images and line profiles. We calculated κ for every point along the simulated approach curves and applied a 20% threshold, where values above this limit were considered inaccurate (Section S13). Logic plots are shown in Figure 3D–F, where red areas indicate inaccurate fitting and blue regions indicate accurate fitting. Single-point fitting is most reliable close to the surface, when $L_{true} < 1$, and becomes dependent on the specific conditions further away. Therefore, accuracy plots for different RG values and accuracy tables are show in the Supporting Information to guide the use of single-point fitting (Sections S14 and S15). QFR has been shown to improve kinetic fitting of approach curves, single points, and when there is an error in the microelectrode area, and this method can be applied to many SECM experiments.

Applying the Single-Point Kinetic Fitting to Line Scans: the Single Redox Mediator Approach. QFR is available in many common experimental conditions and is, in our opinion, underutilized. For instance, studies of electrodes where a noninterfering redox mediator can be added to access positive feedback behavior.[52] Moreover, samples are commonly embedded in inert epoxy or another insulating material that can be used as a negative feedback reference. In this section, we demonstrate and discuss kinetic fitting in the $x-y$ plane of a flat sample, where an active region is embedded in an insulating region acting as a negative feedback reference. Using vacuum-based thin-film deposition techniques, we fabricated a substrate on which Au and SiO_2 line features are arranged in an alternating fashion (Figure 4A), serving as the active and insulating regions, respectively. We have demonstrated previously that these substrates are flat relative to the microelectrode size, which prevents any topography contribution.[46] To suppress the kinetics at the Au–liquid interface, the substrate was exposed to a solution of 1-hexanethiol to form a self-assembled monolayer (SAM), passivating the electrode to reduce charge-transfer kinetics.[53] Surface kinetics were then probed using Ruhex in line with previously studies.[53−55] The diffusion-limited current was measured at different heights over the substrate, and a clear increase in current was measured over the SAM-covered Au regions (Figure 4B). The current reached a plateau over the electroactive area, confirming that the assumption of an infinite substrate in comparison to the microelectrode size was satisfied. Our three-dimensional (3D) simulations show that the active region must be about 5 times the radius of the electrode (Section S16), in line with previous studies.[56] Using the edges of the line scan, which correspond to the insulating SiO_2 strips on the left- and right-hand side, respectively, a linear L profile was generated by interpolating the current and fitting it for L_{calc} . This L profile was used to fit

https://doi.org/10.1021/acs.analchem.2c02498
Anal. Chem. 2022, 94, 13852−13859

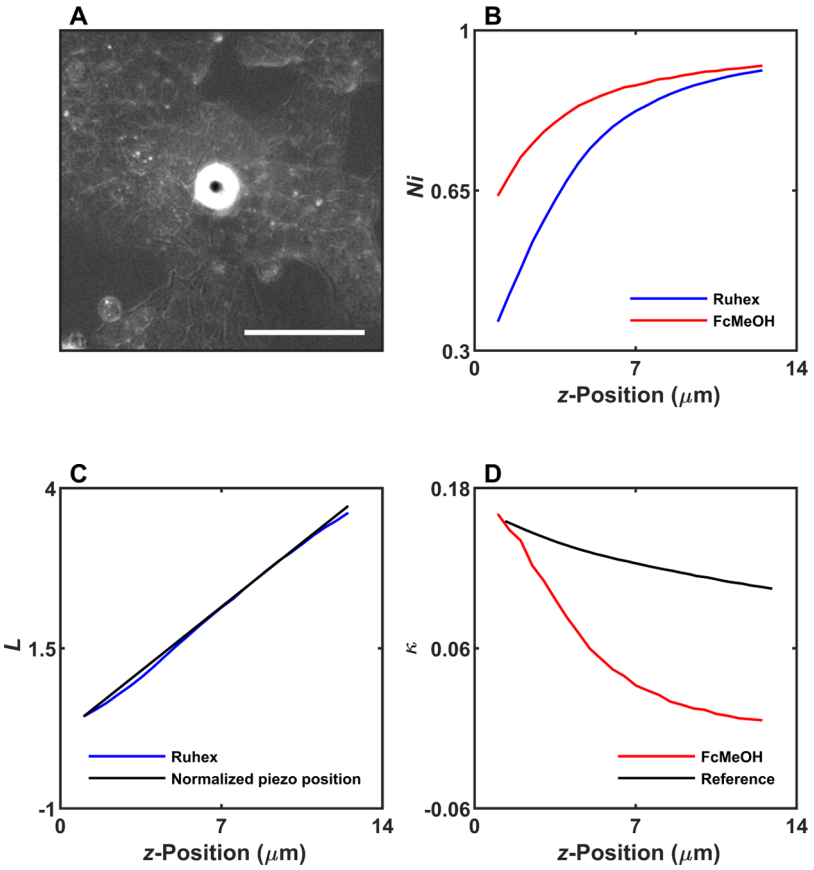

Figure 5. (A) Optical microscopy image of a layer of HEK293 cells adhered to a Zeonor substrate during SECM investigation (view from below). Scale bar: 100 μm. (B) Typical approach curves obtained during FcMeOH oxidation (red line) and Ruhex reduction (blue line). (C) Calculation of the tip-to-substrate distance, L_{calc}, from the Ruhex reduction approach curve (blue line), compared to the normalized piezo extension (black line). (D) Calculation of reaction kinetics, κ_{calc}, from the FcMeOH oxidation approach curve (red line), compared to the curve drawn using the error in the analytical approximations for the value for the closest approach of the FcMeOH curve (black line).

the kinetics along the line scans as shown in Figure 4C. The range of L values of the topography profiles are [0.53, 1.11], well inside the accuracy range seen in Figure 3E. The traces are in good agreement with the kinetics extracted from approach curves measured over the SAM-covered Au. The good agreement between approach curve and line scans shows that the kinetic plane fitting is a reliable strategy, and the accuracy and considerations for this approach have been outlined.

Preferential Redox Mediator Response of the Cell Membrane: the Dual Redox Mediator Approach. The electrochemical response of cells is an important topic in Bio-SECM, and early studies found that charged bulky redox mediators are impermeable to the cell membrane, providing a negative topography reference.[18,19] Dual-mediator systems, such as $O_2/K_4Ru(CN)_6$ and FcMeOH/Ruhex,[20,21] are often employed where one redox mediator is sensitive to topography and the another is sensitive to the cell property of interest. We utilized the FcMeOH/Ruhex dual-mediator system to deconvolute topography and reactivity over HEK293 cell monolayers (Figure 5A). An approach protocol was implemented, similar to the voltage-switching mode introduced by Takahasi et al.,[38] where the approach was carried out at +350 mV (FcMeOH oxidation) and the retract at -350 mV (Ruhex reduction). A clear difference in the approach curves is observed between FcMeOH and Ruhex (Figure 5B), where the FcMeOH approach curve shows a higher current than Ruhex, in line with previous studies of cellular FcMeOH regeneration[12,43] and cell permeability.[57,58] The Ruhex approach curve was used to calculate L according to the QFR method, which agrees well with the normalized piezo extension (Figure 4C). The cell layer thus behaves approximately as a flat substrate with respect to the probe size. The approach curve was repeatable as shown in the Supporting Information (Section S17). The quantitative negative feedback response allows the assessment of the cell kinetics using FcMeOH currents. We then used L_{calc} to fit κ along the FcMeOH approach curve (Figure 5D). A clear decay in the kinetic constant sheds light on the response toward FcMeOH. Although such a decay is expected from the small errors in the analytical approximations (black line), the deviation is more substantial, indicating that the cell permeability is perturbing kinetic measurements to some extent. The permeability of the cell membrane to FcMeOH needs to be accounted for as pointed out in previous studies.[20] The QFR methods allow quick identification and analysis of the cellular response to clearly show when permeability effects are present and substantial without resorting to numerical simulations. An increase in cell permeability is a first step in cell damage that occurs in cells when exposed to toxic heavy metals,[57,59,60] surfactants,[61] or by the removal of the controlled cell culture atmosphere,[43] which can occur during normal Bio-SECM studies. However, such stress also results in release of the cell contents, which can influence the current response.[43] Dual-mediator systems and QFR can be a useful approach to more complex analysis of the

https://doi.org/10.1021/acs.analchem.2c02498
Anal. Chem. 2022, 94, 13852−13859

effect of permeability by referencing to the current of a noninteracting mediator such as Ruhex and an interacting mediator such as FcMeOH[58] to study extracellular species and membrane-confined structures.

CONCLUSIONS

We have demonstrated that negative and positive feedback currents can be used for improved fitting of SECM measurements through calculating the tip-to-substrate distance directly, named herein quantitative feedback referencing (QFR). Two examples were highlighted for using the developed framework: deconvolution of negative feedback for flat samples in a spatially controlled fashion and using the preferential response of the cell membrane toward a cell impermeable redox mediator. We exemplified this analysis through first-order irreversible kinetics, but any simulation or derived data can be used. The QFR framework is applicable to single-point fitting of images and is less influenced by experimental errors and fitting subjectivity, which brings us closer to fulfilling the analytical figures of merit for SECM analysis, reliable downscaling, and improving its accessibility and reproducibility. We envision that the method can be integrated into currently available scanning probe microscopy software for improved positioning and automation.

ASSOCIATED CONTENT

Supporting Information

The Supporting Information is available free of charge at https://pubs.acs.org/doi/10.1021/acs.analchem.2c02498.

Simulation geometry and mesh figures; additional experimental information on the finite element model; table providing simulation overview; analytical approximations; fitting procedures; table providing accuracy of *L*-fitting by negative feedback; table providing accuracy of *L*-fitting by positive feedback; approach curve κ-fitting methods; figures showing the effect of RG on approach curve fitting; table providing accuracy of fitting entire approach curves; figures and table showing accuracy of fitting entire approach curves with error in the microelectrode area; single-point κ-fitting; figures showing the effect of RG on single-point κ-fitting; table providing accuracy of single-point κ-fitting; figures showing line scan simulations; and figures showing repeatability of cell measurements (PDF)

AUTHOR INFORMATION

Corresponding Author

Janine Mauzeroll − *Department of Chemistry, McGill University, Montreal, Quebec H3A 0B8, Canada;* orcid.org/0000-0003-4752-7507; Email: janine.mauzeroll@mcgill.ca

Authors

Sebastian Amland Skaanvik − *Department of Chemistry, McGill University, Montreal, Quebec H3A 0B8, Canada;* orcid.org/0000-0002-5302-8221

Lisa Irene Stephens − *Department of Chemistry, McGill University, Montreal, Quebec H3A 0B8, Canada;* orcid.org/0000-0002-0064-7555

Samantha Michelle Gateman − *Department of Chemistry, University of Western Ontario, London, Ontario N6A 3K7, Canada*

Matthias Geissler − *Life Sciences Division, National Research Council of Canada, Boucherville, Quebec J4B 6Y4, Canada;* orcid.org/0000-0002-8838-5528

Complete contact information is available at: https://pubs.acs.org/10.1021/acs.analchem.2c02498

Notes

The authors declare no competing financial interest.

ACKNOWLEDGMENTS

J.M. acknowledges funding from the NSERC Discovery program (grant #RGPIN-2020-04609).

REFERENCES

(1) Bard, A. J.; Fan, F. R. F.; Kwak, J.; Lev, O. *Anal. Chem.* **1989**, *61*, 132−138.
(2) Polcari, D.; Dauphin-Ducharme, P.; Mauzeroll, J. *Chem. Rev.* **2016**, *116*, 13234−13278.
(3) Gateman, S. M.; Stephens, L. I.; Perry, S. C.; Lacasse, R.; Schulz, R.; Mauzeroll, J. *npj Mater. Degrad.* **2018**, *2*, No. 5.
(4) Payne, N. A.; Stephens, L. I.; Mauzeroll, J. *Corrosion* **2017**, *73*, 759−780.
(5) Bertoncello, P. *Energy Environ. Sci.* **2010**, *3*, 1620−1633.
(6) Byers, J. C.; Güell, A. G.; Unwin, P. R. *J. Am. Chem. Soc.* **2014**, *136*, 11252−11255.
(7) Rincón, R. A.; Ventosa, E.; Tietz, F.; Masa, J.; Seisel, S.; Kuznetsov, V.; Schuhmann, W. *ChemPhysChem* **2014**, *15*, 2810−2816.
(8) Cannan, S.; Cervera, J.; Steliaros née Haskins, R. J.; Bitziou, E.; Whitworth, A. L.; Unwin, P. R. *Phys. Chem. Chem. Phys.* **2011**, *13*, 5403−5412.
(9) McGeouch, C.-A.; Peruffo, M.; Edwards, M. A.; Bindley, L. A.; Lazenby, R. A.; Mbogoro, M. M.; McKelvey, K.; Unwin, P. R. *J. Phys. Chem. C* **2012**, *116*, 14892−14899.
(10) Burchardt, M.; Wittstock, G. *Bioelectrochemistry* **2008**, *72*, 66−76.
(11) Liu, B.; Rotenberg, S. A.; Mirkin, M. V. *Proc. Natl. Acad. Sci. U.S.A.* **2000**, *97*, 9855−9860.
(12) Rapino, S.; Marcu, R.; Bigi, A.; Soldà, A.; Marcaccio, M.; Paolucci, F.; Pelicci, P. G.; Giorgio, M. *Electrochim. Acta* **2015**, *179*, 65−73.
(13) Petroniene, J.; Morkvenaite-Vilkonciene, I.; Miksiunas, R.; Bironaite, D.; Ramanaviciene, A.; Rucinskas, K.; Janusauskas, V.; Ramanavicius, A. *Electrochim. Acta* **2020**, *360*, No. 136956.
(14) Engstrom, R. C.; Small, B.; Kattan, L. *Anal. Chem.* **1992**, *64*, 241−244.
(15) Eckhard, K.; Chen, X.; Turcu, F.; Schuhmann, W. *Phys. Chem. Chem. Phys.* **2006**, *8*, 5359−5365.
(16) Zoski, C. G.; Aguilar, J. C.; Bard, A. J. *Anal. Chem.* **2003**, *75*, 2959−2966.
(17) Etienne, M.; Schulte, A.; Schuhmann, W. *Electrochem. Commun.* **2004**, *6*, 288−293.
(18) Wipf, D. O.; Bard, A. J. *Anal. Chem.* **1992**, *64*, 1362−1367.
(19) Cornut, R.; Lefrou, C. *J. Electroanal. Chem.* **2008**, *621*, 178−184.
(20) Cornut, R.; Lefrou, C. *J. Electroanal. Chem.* **2007**, *608*, 59−66.
(21) Lefrou, C. *J. Electroanal. Chem.* **2006**, *592*, 103−112.
(22) Cornut, R.; Griveau, S.; Lefrou, C. *J. Electroanal. Chem.* **2010**, *650*, 55−61.
(23) Holzinger, A.; Steinbach, C.; Kranz, C. Scanning Electrochemical Microscopy (SECM): Fundamentals and Applications in Life Sciences. In *Electrochemical Strategies in Detection Science*, Arrigan, D. W. M., Ed.; The Royal Society of Chemistry, 2016; Chapter 4, Vol. *125*.
(24) Lee, Y.; Ding, Z.; Bard, A. J. *Anal. Chem.* **2002**, *74*, 3634−3643.

(25) Takahashi, K.; Shibata, T.; Oba, T.; Ishikawa, T.; Yoshikawa, M.; Tatsunami, R.; Takahashi, K.; Tampo, Y. *Life Sci.* **2009**, *84*, 211−217.
(26) Cougnon, C.; Bauer-Espindola, K.; Fabre, D. S.; Mauzeroll, J. *Anal. Chem.* **2009**, *81*, 3654−3659.
(27) Alpuche-Aviles, M. A.; Wipf, D. O. *Anal. Chem.* **2001**, *73*, 4873−4881.
(28) Gabrielli, C.; Huet, F.; Keddam, M.; Rousseau, P.; Vivier, V. *J. Phys. Chem. B* **2004**, *108*, 11620−11626.
(29) MKelvey, K.; Edwards, M. A.; Unwin, P. R. *Anal. Chem.* **2010**, *82*, 6334−6337.
(30) Lazenby, R. A.; McKelvey, K.; Unwin, P. R. *Anal. Chem.* **2013**, *85*, 2937−2944.
(31) Macpherson, J. V.; Unwin, P. R. *Anal. Chem.* **2001**, *73*, 550−557.
(32) Macpherson, J. V.; Unwin, P. R. *Anal. Chem.* **2000**, *72*, 276−285.
(33) Kueng, A.; Kranz, C.; Lugstein, A.; Bertagnolli, E.; Mizaikoff, B. *Angew. Chem., Int. Ed.* **2003**, *42*, 3238−3240.
(34) Bergner, S.; Vatsyayan, P.; Matysik, F.-M. *Anal. Chim. Acta* **2013**, *775*, 1−13.
(35) Ciocci, P.; Lemineur, J.-F.; Noël, J.-M.; Combellas, C.; Kanoufi, F. *Electrochim. Acta* **2021**, *386*, No. 138498.
(36) Griveau, S.; Aroua, S.; Bediwy, D.; Cornut, R.; Lefrou, C.; Bedioui, F. *J. Electroanal. Chem.* **2010**, *647*, 93−96.
(37) Unwin, P. R.; Bard, A. J. *J. Phys. Chem. A* **1991**, *95*, 7814−7824.
(38) Takahashi, Y.; Shevchuk, A. I.; Novak, P.; Babakinejad, B.; Macpherson, J.; Unwin, P. R.; Shiku, H.; Gorelik, J.; Klenerman, D.; Korchev, Y. E.; Korchev, Y. E.; Matsue, T. *Proc. Natl. Acad. Sci. U.S.A.* **2012**, *109*, 11540−11545.
(39) Lhenry, S.; Leroux, Y. R.; Hapiot, P. *Anal. Chem.* **2013**, *85*, 1840−1845.
(40) Souto, R. M.; Fernández-Mérida, L.; González, S. *Electroanalysis* **2009**, *21*, 2640−2646.
(41) Kuss, S.; Polcari, D.; Geissler, M.; Brassard, D.; Mauzeroll, J. *Proc. Natl. Acad. Sci. U.S.A.* **2013**, *110*, 9249−9254.
(42) Kuss, S.; Cornut, R.; Beaulieu, I.; Mezour, M. A.; Annabi, B.; Mauzeroll, J. *Bioelectrochemistry* **2011**, *82*, 29−37.
(43) Polcari, D.; Hernández-Castro, J. A.; Li, K.; Geissler, M.; Mauzeroll, J. *Anal. Chem.* **2017**, *89*, 8988−8994.
(44) Cornut, R.; Bhasin, A.; Lhenry, S.; Etienne, M.; Lefrou, C. *Anal. Chem.* **2011**, *83*, 9669−9675.
(45) Anicet, N.; Bourdillon, C.; Moiroux, J.; Savéant, J.-M. *J. Phys. Chem. B* **1998**, *102*, 9844−9849.
(46) Stephens, L. I.; Payne, N. A.; Skaanvik, S. A.; Polcari, D.; Geissler, M.; Mauzeroll, J. *Anal. Chem.* **2019**, *91*, 3944−3950.
(47) Danis, L.; Polcari, D.; Kwan, A.; Gateman, S. M.; Mauzeroll, J. *Anal. Chem.* **2015**, *87*, 2565−2569.
(48) Beaulieu, I.; Geissler, M.; Mauzeroll, J. *Langmuir* **2009**, *25*, 7169−7176.
(49) Cornut, R.; Lefrou, C. *J. Electroanal. Chem.* **2008**, *623*, 197−203.
(50) Cornut, R.; Hapiot, P.; Lefrou, C. *J. Electroanal. Chem.* **2009**, *633*, 221−227.
(51) Moussa, S.; Mauzeroll, J. *J. Electrochem. Soc.* **2019**, *166*, G25−G38.
(52) Sun, T.; Wang, D.; Mirkin, M. V.; Cheng, H.; Zheng, J.-C.; Richards, R. M.; Lin, F.; Xin, H. L. *Proc. Natl. Acad. Sci.* **2019**, *116*, 11618−11623.
(53) Liu, B.; Bard, A. J.; Mirkin, M. V.; Creager, S. E. *J. Am. Chem. Soc.* **2004**, *126*, 1485−1492.
(54) Forouzan, F.; Bard, A. J.; Mirkin, M. V. *Isr. J. Chem.* **1997**, *37*, 155−163.
(55) Salamifar, S. E.; Mehrgardi, M. A.; Kazemi, S. H.; Mousavi, M. F. *Electrochim. Acta* **2010**, *56*, 896−904.
(56) Bard, A. J.; Mirkin, M. V.; Unwin, P. R.; Wipf, D. O. *J. Phys. Chem. B* **1992**, *96*, 1861−1868.
(57) Li, M. S. M.; Filice, F. P.; Ding, Z. *J. Inorg. Biochem.* **2014**, *136*, 177−183.
(58) Bergner, S.; Wegener, J.; Matysik, F.-M. *Anal. Methods* **2012**, *4*, 623−629.
(59) Henderson, J. D.; Filice, F. P.; Li, M. S. M.; Ding, Z. *ChemElectroChem* **2017**, *4*, 856−863.
(60) Li, M. S. M.; Filice, F. P.; Henderson, J. D.; Ding, Z. *J. Phys. Chem. C* **2016**, *120*, 6094−6103.
(61) Koley, D.; Bard, A. J. *Proc. Natl. Acad. Sci. U.S.A.* **2010**, *107*, 16783−16787.

Recommended by ACS

Fitting Kinetics from Scanning Electrochemical Microscopy Images of Finite Circular Features
Nathaniel Leslie, Janine Mauzeroll, *et al.*
OCTOBER 25, 2022
ANALYTICAL CHEMISTRY
READ

Controlling Surface Contact, Oxygen Transport, and Pitting of Surface Oxide via Single-Channel Scanning Electrochemical Cell Microscopy
Yuanjiao Li, Janine Mauzeroll, *et al.*
OCTOBER 10, 2022
ANALYTICAL CHEMISTRY
READ

Wireless Imaging of Transient Redox Activity Based on Bipolar Light-Emitting Electrode Arrays
Gerardo Salinas, Alexander Kuhn, *et al.*
OCTOBER 03, 2022
ANALYTICAL CHEMISTRY
READ

On-Demand Electrochemical Fabrication of Ordered Nanoparticle Arrays using Scanning Electrochemical Cell Microscopy
Md. Maksudur Rahman, Caleb M. Hill, *et al.*
NOVEMBER 18, 2022
ACS NANO
READ

Get More Suggestions >

https://doi.org/10.1021/acs.analchem.2c02498
Anal. Chem. 2022, 94, 13852−13859